processes

MDPI

*Article*

# The Pore Structure Development and Evolution of the Q4 Member in Lower Cretaceous, Northern Songliao Basin

**Junhui Li [1], Fangju Chen [1,2,*], Qiang Zheng [1], Yanping Zhu [1], Qi Wang [1] and Jiawei Hao [1]**

[1] Exploration and Development Research Institute of PetroChina Daqing Oilfield Company Limited, Daqing 163712, China; yjylijh@petrochina.com.cn (J.L.); zhengqiang2022@petrochina.com.cn (Q.Z.); zhuyanping@petrochina.com.cn (Y.Z.); wangqi1990@petrochina.com.cn (Q.W.); haojue99@petrochina.com.cn (J.H.)
[2] School of Earth Sciences, Northeast Petroleum University, Daqing 163318, China
* Correspondence: chenfangju@petrochina.com.cn

**Abstract**

To better characterize the pore development and evolution characteristics in the fourth member of the Quantou Formation (Q4), an accurate evaluation of the reservoir properties and oiliness for different types of reservoirs was conducted in this study. Polarization microscope and scanning electron microscope experiments were used for lithology, mineral composition, pore types, and morphology observation. High-pressure mercury intrusion experiments were used to characterize the porosity, permeability, and pore size distribution, and the Beard and Weyl model was used to calculate the porosity evolution characteristics. The results reveal the following: (i) siltstone and pelitic siltstone dominate the Q4 tight reservoir, while feldspar and quartz are the main rock-forming minerals. (ii) Intergranular pores, intergranular dissolution pores, intragranular dissolution pores, intercrystalline pores, and microfractures are the main pore types, with a porosity of 4% to 12% and a permeability of 0.001 to 1 mD. (iii) After the Q4 reservoir was divided into Grade I, II, and II reservoirs from good to poor, their current average porosity values were found to be 14.82%, 8.98%, and 3.57%, respectively. The results from this work are of great significance for accumulation space and oiliness evaluation, and they provide theoretical support for the exploitation of Q4 tight reservoirs in the study area.

**Keywords:** pore structure; porosity and permeability; pore evolution; diagenesis

check for updates

Academic Editor: Chuanliang Yan

Received: 5 November 2025
Revised: 1 December 2025
Accepted: 5 December 2025
Published: 8 December 2025

**Citation:** Li, J.; Chen, F.; Zheng, Q.; Zhu, Y.; Wang, Q.; Hao, J. The Pore Structure Development and Evolution of the Q4 Member in Lower Cretaceous, Northern Songliao Basin. *Processes* **2025**, *13*, 3965. https://doi.org/10.3390/pr13123965

**Copyright:** © 2025 by the authors. Licensee MDPI, Basel, Switzerland. This article is an open access article distributed under the terms and conditions of the Creative Commons Attribution (CC BY) license (https://creativecommons.org/licenses/by/4.0/).

## 1. Introduction

Tight oil and gas pertain to the field of unconventional energy, and researchers have made significant breakthroughs in exploration theory, development technology, and industrial application in recent years [1,2]. However, there are significant differences in production at different wells in the exploration and development practices of the Ordos Basin, Sichuan Basin, and Songliao Basin [3,4]. Low porosity and low permeability are the prominent features of tight reservoirs, and their complex pore structure and strong heterogeneity lead to a complex accumulation mechanism [5,6]. Based on the occurrence space, interaction intensity with pore walls, and mobility, the tight reservoir is divided into adsorbed and free hydrocarbons [7,8], which makes it difficult to accurately evaluate the oiliness and mobility. The precise evaluation of porosity, permeability, pore size distribution, and evolution characteristics is the foundation of the above research. Liu and Zhang [9] observed five pore types of residual intergranular pores, intergranular dissolution pores, intragranular dissolution pores, clay mineral intercrystalline pores, and microfractures in the $Q_4$ reservoir,

which has the characteristics of thin pore throat and worse pore structure. Moreover, the $Q_4$ reservoir was divided into five lithofacies, where the feldspar dissolution pore lithofacies with moderate compaction and strong dissolution and residual intergranular pore lithofacies with weak compaction and moderate cementation were deemed as the best $Q_4$ reservoir in the study area; the residual intergranular pore lithofacies with moderate compaction and cementation was secondary; the matrix intergranular pore lithofacies with weak compaction and cementation and the intercrystalline micropores lithofacies of weak compaction and strong cementation performed worse. Ran et al. [10] investigated the accumulation conditions of the $Q_4$ reservoir in the Putaohua Oilfield, northern Songliao Basin, and suggested that the porosity of a high-quality reservoir should be higher than 10%. Ma et al. [11] conducted nuclear magnetic resonance to characterize the pore structure of the $Q_4$ reservoir in the Xinmiao Oilfield, and their results indicated that pore throat radius is in the range of 0.2–6 μm and controls its permeability and pore connectivity. In addition, they divided the pores into two types: big pore–thin throat and small pore–thick throat.

Overall, the $Q_4$ reservoir of the Upper Cretaceous in the Songliao Basin has diverse pore types, wide pore size distribution, varying connectivity, and significant differences in porosity and permeability [12,13]. Therefore, the spatiotemporal evolution of accumulation capacity, oil content, and mobility is complex under the constraints of lateral and interlayer heterogeneity of the reservoir, which influences the accurate prediction of production. In particular, the evolution law of pore structure under the differential influence of various diagenesis is unclear. However, there are significant diagenesis differences with respect to the Q4 reservoir in the Songliao Basin, which mainly include the early diagenetic stage, A period of the middle diagenetic stage, and B period of the middle diagenetic stage [14–16]. Under the constraint of differential diagenetic evolution, pore structure and oil content evolution characteristics and mechanisms of reservoirs are unclear, resulting in a lack of theoretical support for oiliness and accumulation capacity evaluation [17–19]. As a result, the exploration and development effects of some wells are far away expectations [20,21]. Therefore, it is necessary to clarify the differential diagenesis of the Q4 reservoir in the study area and evaluate it according to various grades based in their exploitation potential. In this work, a total of 27 $Q_4$ reservoir samples were collected from the northern Songliao Basin; the polarization microscope and scanning electron microscope were employed for the observation of lithofacies, mineral composition, pore type, and diagenesis; a high-pressure mercury intrusion porosimeter was employed to quantitatively characterize the pore structure development. Then, the impacts of compaction, cementation, and dissolution on porosity were calculated according to the Beard and Weyl model [22], and the pore evolution pattern was established accordingly. As a result, the $Q_4$ reservoir was divided into three grades of I, II, and III from good to poor. The results from this work could provide theoretical references for the research on the pore structure and evolution characteristics of the $Q_4$ reservoir in the Songliao Basin.

## 2. Experiments and Methods

### *2.1. Optics and Fluid Injection Experiments*

A total of 27 $Q_4$ reservoir of Upper Cretaceous samples were collected from the northern Songliao Basin, which was deposited in shallow water delta system [15,23,24]. The lithology is mainly composed of fine sandstone, siltstone, and pelitic siltstone. A Leica (Wetzlar, Germany) DM2700P polarization microscope was employed for microsection observation (Table 1). Prior to experiments, (i) a cylindrical sample with a diameter of 20 mm was drilled to cut and bond glass slide; (ii) the dyed liquid was injected into the pore structure of sample under a pressure difference of 0.5–1.2 MPa to ensure complete filling of microscale pores; (iii) the liquid glue was subjected to polymerization and solidification

treatment under 60 °C for 24 h; (iv) the samples were ground to a standard thickness of 30 μm for better exhibition of the pore stained areas. A ZEISS (Oberkochen, Germany) SIGMA03040100 scanning electron microscope was used for the clay mineral pores observation, and a Micromeritics (Norcross, GA, USA) Auto Pore V9620 high-pressure mercury intrusion porosimeter was employed for the quantitative analysis of pore structure.

**Table 1.** The experimental equipment for microsection observation, pore observation, and pore size, porosity, and permeability measurement.

| Experimental Item | Experimental Equipment |
| --- | --- |
| Microsection observation | DM2700P Polarization Microscope |
| Pore observation | SIGMA03040100 Scanning Electron Microscope |
| Pore size, porosity, and permeability | Auto Pore V9620 High-Pressure Mercury Intrusion Porosimeter |

### *2.2. The Calculation Methods of Porosity Changes*

The porosity calculation in this work comprises original, compaction loss, cementation loss, and dissolution increase porosity according to the research of Beard and Weyl [22]. It is a simplified model based on the influence of compaction and cementation on reservoir porosity, which follows the following assumptions: (i) the porosity decreases exponentially with depth, ignoring secondary pore formation mechanisms; (ii) the difference between early, middle, and late diagenesis is not distinguished. Therefore, this model is only suitable for homogeneous sandstone reservoirs and has a large prediction error for complex diagenetic environments.

(1) The calculation of original porosity

$$\Phi_0 = 20.91 + 22.9/S_0 \tag{1}$$

$$S_0 = \sqrt{\frac{D_1}{D_3}} \tag{2}$$

$\Phi_0$ is the original porosity, $S_0$ is the Trask sorting coefficient, and $D_1$ and $D_3$ are the particle diameters (μm) corresponding to 25% and 75% on the cumulative curve, respectively.

(2) The calculation of compaction loss porosity

$$\Phi_1 = \mathrm{C_t} + \left[\frac{(\Phi_{pm} + \Phi_{d1})\Phi_p}{\Phi_T}\right] \tag{3}$$

$$\Phi_L = \Phi_0 - \Phi_1 \tag{4}$$

$\Phi_1$ is the porosity after compaction; $\Phi_L$, $\Phi_p$, $\Phi_t$, $\Phi_{pm}$, and $\Phi_{d1}$ are physical property analysis porosity, total surface porosity, primary surface porosity, and dissolution surface porosity of intergranular dissolution pores, respectively; $\mathrm{C_t}$ is the current cement content.

(3) The calculation of cementation loss porosity

$$\Phi_2 = \left(\frac{\Phi_{pm}}{\Phi_t}\right)\Phi_p \tag{5}$$

$$\Phi_c = \Phi_1 - \Phi_2 \tag{6}$$

$\Phi_2$ is the porosity after cementation, and $\Phi_c$ is the cementation loss porosity.

(4) The calculation of dissolution increase porosity

$$\Phi_3 = (\Phi_{d1} + \Phi_{d2})\Phi_p/\Phi_t \tag{7}$$

$\Phi_2$ is the dissolution increase porosity, and $\Phi_{d2}$ is the dissolution surface porosity of intragranular dissolution pores.

## 3. Results and Discussion

### *3.1. Physical Properties of $Q_4$ Reservoir*

(1) Mineralogical composition of $Q_4$ reservoir

The lithology of the $Q_4$ reservoir in the study area is mainly composed of siltstone and pelitic siltstone, with fine grain size belonging to tight reservoirs. Feldspar and quartz are the main rock-forming minerals, also including a certain amount of rock debris (Figures 1 and 2). Therefore, rock debris–feldspar siltstone is the main rock type, followed by feldspar–rock debris siltstone and rock debris siltstone. Among them, feldspar contributes about 30%, with the content of potassium feldspar being slightly larger than plagioclase (Figure 1). Rock debris is dominated by igneous and metamorphic rock debris, with the former having the characteristics of high hardness and low porosity. Consequently, a higher igneous debris usually results in a worse porosity, which will further influence the permeability and accumulation capacity of the reservoir. As particularly noted in Figure 2g–l, the pores among quartz and feldspar particles are generally filled by rock debris. There is a significant impact of mineral composition on the reservoir properties, where the contents of quartz and feldspar mostly correlated positively with the reservoir properties and were deemed as the material basis of tight reservoirs [25,26]. The main reason is that both of them have high mechanical strength and strong resistance to compaction, and the primary pores can be well preserved during diagenesis [27,28]. In addition, there is also a large amount of dissolution pores on the feldspar surface (Figure 1a,b and Figure 2a,b,h).

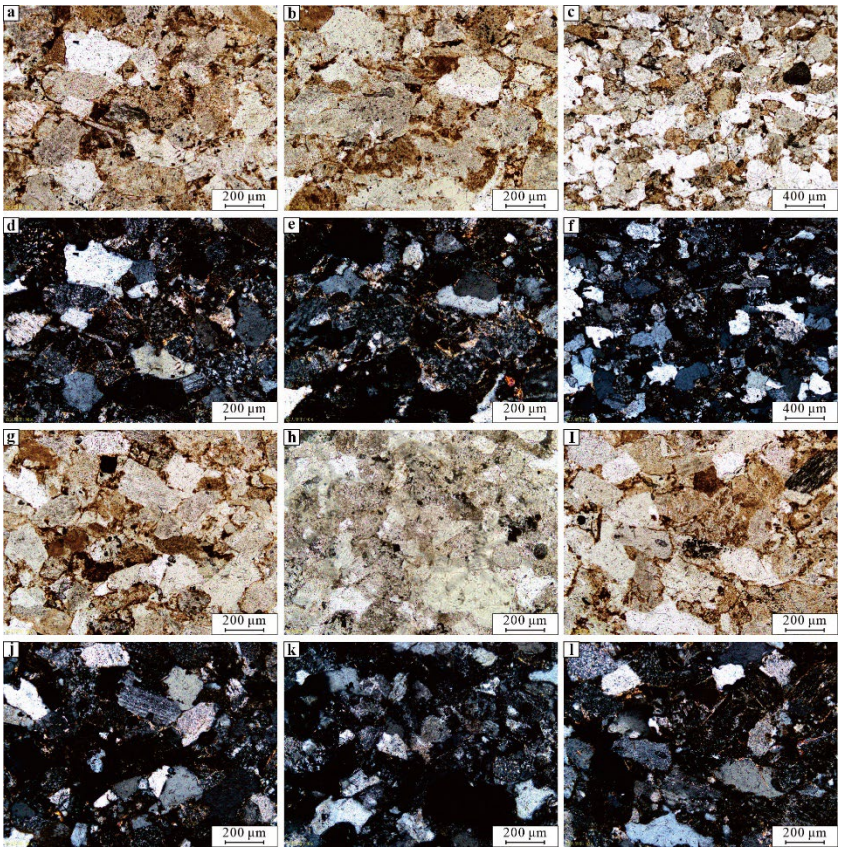



**Figure 1.** The development of quartz, feldspar, and rock debris in $Q_4$ reservoir. (**a**–**g**): the rock debris–feldspar siltstone, also including a small amount of muscovite. (**h**–**l**): double crystal can be identified on the feldspar surface and was generally dissolved.

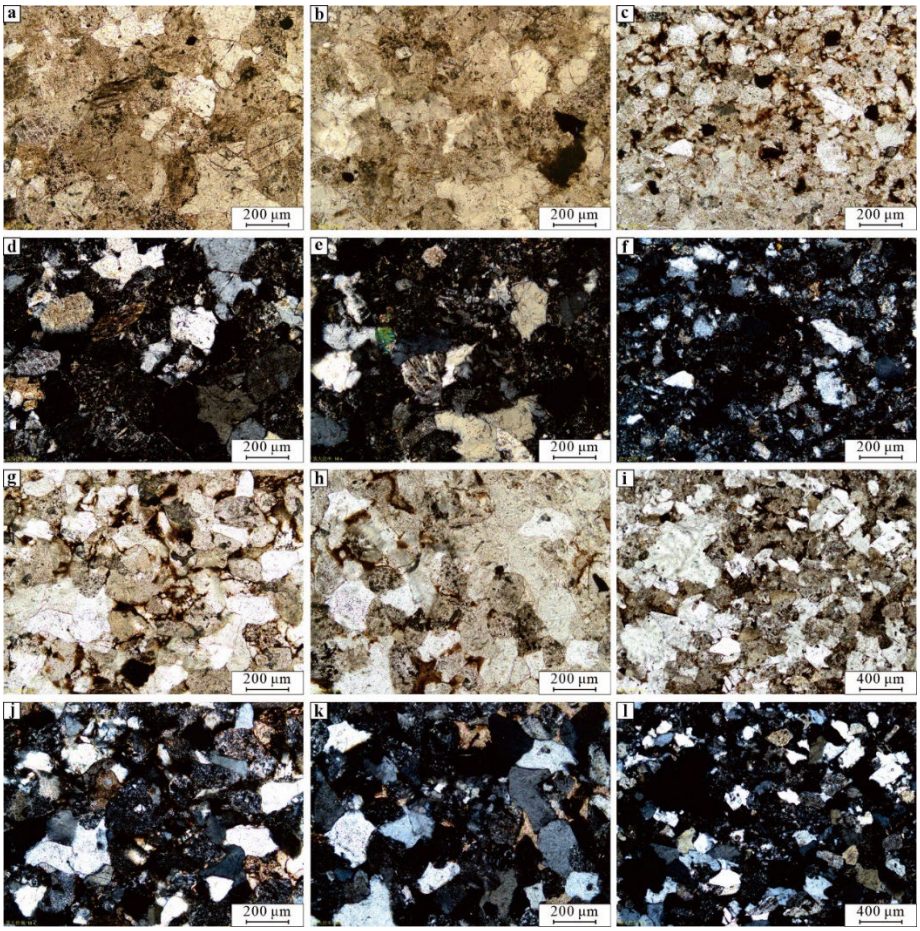



**Figure 2.** The development of quartz and debris in $Q_4$ reservoir. (**a**–**f**) are feldspar–rock debris siltstone, and (**g**–**l**) are mainly debris siltstone. Igneous debris is the main debris type, and there is also a small amount of muscovite.

In addition to the mineral particles, there are also some interstitial materials which comprise a relative content of about 10%. Among them, the content of muddy matrix (mainly illite clay minerals) is the highest accounting for about a half, followed by carbonate (mainly calcite and dolomite minerals) cement (Figure 3). High contents of matrix and cement occupy the accumulation space, blocking pore channels and leading to reservoir densification. In tight siltstone reservoirs, the dissolution of cement such as calcite and dolomite is crucial for affecting the development of secondary pores and improving reservoir capacity. However, the influence of carbonate content is reflected in three aspects: (i) it filled the pores and resulted in the reduction of porosity; (ii) it resisted mechanical compaction and protected the primary pores to some extent; (iii) its dissolution formed a certain amount of secondary pores. For clay minerals, they were usually deemed as negative factors for the forming and preservation of pores [29,30].

(2) Porosity and permeability of $Q_4$ reservoir

Porosity and permeability are the significant evaluation indices for the accumulation and seepage capacity of tight reservoirs [31,32]. The porosity of the $Q_4$ reservoir ranges from 4% to 12%, with an average of 8.37%; and its permeability is in the range of 0.001–1 mD, with an average of 0.042 mD. Among them, the reservoir with a porosity of 5–15% accounts the largest proportion (48%), followed by the reservoirs in 10–15% (33%) and <5% (19%); the permeability of the $Q_4$ reservoirs is mostly lower than 0.1 mD, with a proportion of 85%, and only the remaining 15% are larger than 0.1 mD (Figure 4) Therefore, the $Q_4$ siltstone in the study area belongs mostly to the low porosity and ultralow permeability reservoir category, and the physical properties perform worse.

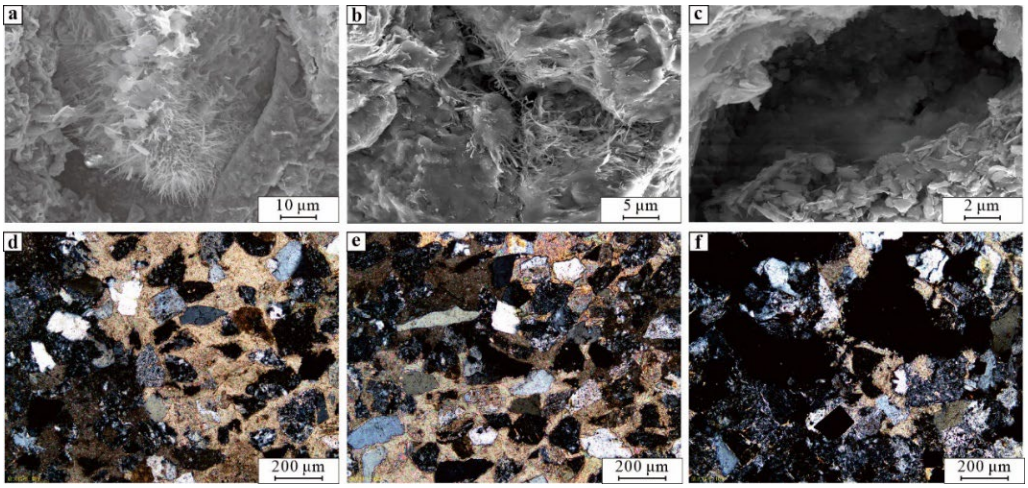



**Figure 3.** The development of clay minerals and carbonate minerals in $Q_4$ reservoir. (**a**–**c**) are the illite clay minerals filled into the intergranular pores; (**d**–**f**) are the carbonate minerals filled into the intergranular pores.

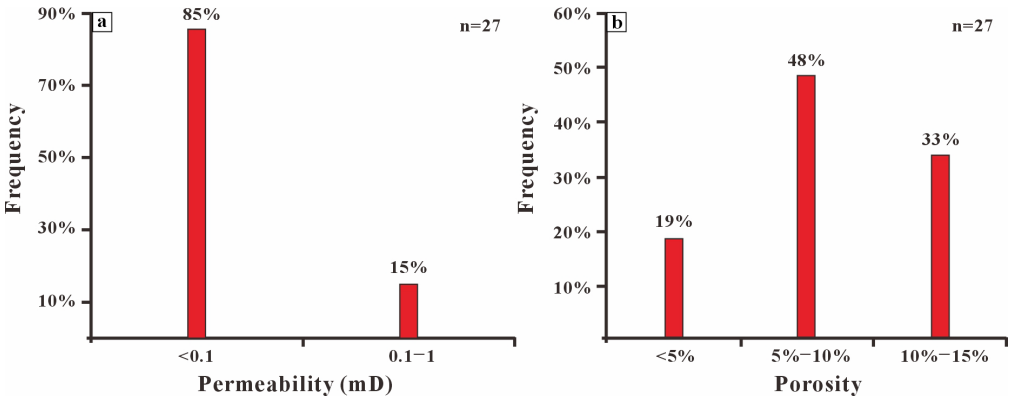



**Figure 4.** The distribution of permeability (**a**) and porosity (**b**) of $Q_4$ reservoir.

### *3.2. The Development of Pore Types in $Q_4$ Reservoir*

Pores in the tight reservoir were divided into primary and secondary pores [33,34]. In the $Q_4$ reservoir, the former mainly refers to intergranular pores remaining from compaction and cementation, and the latter consists mainly of dissolution pores and mold pores. To better characterize the developmental characteristics of various types of pores, they were further divided into intergranular pores, intergranular dissolution pores, intragranular dissolution pores, intercrystalline pores, and microfractures.

(1) The development of intergranular pores

The intergranular pores were formed during the initial sedimentation process and were the pores left behind by the compaction and cementation effects of later diagenesis. They mostly developed in reservoirs with high content of brittle minerals such as quartz and feldspar (Figure 5a–c) due to their resistance to mechanical compaction. The pores are mostly in triangular or polygonal shapes, with straight edges and clean interiors without obvious signs of dissolution; and the pore size is relatively small, ranging from 50 μm to 100 μm.

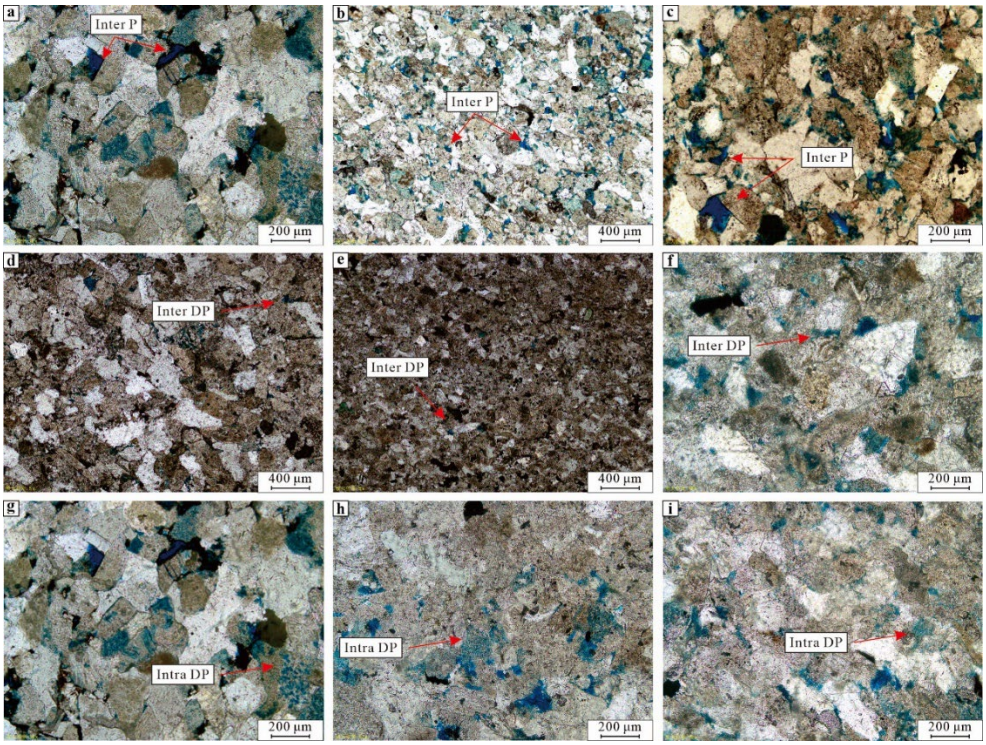



**Figure 5.** The development characteristics of intergranular pores (Inter P), intergranular dissolution pores (Inter DP), and intragranular pores in $Q_4$ reservoir (Intra P). (**a**–**c**) are intergranular pores; (**d**–**f**) are intergranular dissolution pores; and (**g**–**i**) are intragranular pores.

(2) Intergranular dissolution pores and intragranular dissolution pores

In the $Q_4$ reservoir, the intergranular dissolution pores formed by the dissolution of feldspar and rock debris are the most common (Figure 5d–f). Their formation originates from intergranular pores and feldspar mold pores caused by the dissolution of feldspar edges. After dissolution, the feldspar edges appear in a harbor or irregular shape, with pore diameters generally ranging from 100 μm to 150 μm. Intragranular dissolution pores are developed inside the minerals rather than the edges. Strong local dissolution is their main cause. There are a large number of intragranular dissolution pores in the $Q_4$ reservoir, which are usually irregular in shape, with pore sizes ranging from 100 μ m to 200 μm (Figure 5g–i), and that have poor connectivity. In particular, feldspar dissolution is significant in some areas, and the particles are seriously dissolved, resulting in mold pores.

(3) Clay mineral pores and microfractures

Clay mineral pores were formed due to the filling of authigenic clay minerals (Figure 6a,b), including kaolinite, mixed I/S, illite, and chlorite intercrystalline pores. Nanoscale pores dominate the pore size, resulting in pore connectivity. The contribution of microfractures to the pore structure in the $Q_4$ reservoir is about 3%, with their length measured at the micro scale and width at the nano scale (Figure 6c,d). The diagenetic shrinkage effect and compaction effect of clay minerals are their main causes, resulting in the development of microfractures of clay and brittle minerals. Overall, accumulation space of the $Q_4$ reservoir is mainly composed of residual intergranular pores, intergranular dissolution pores, and intragranular dissolution pores.

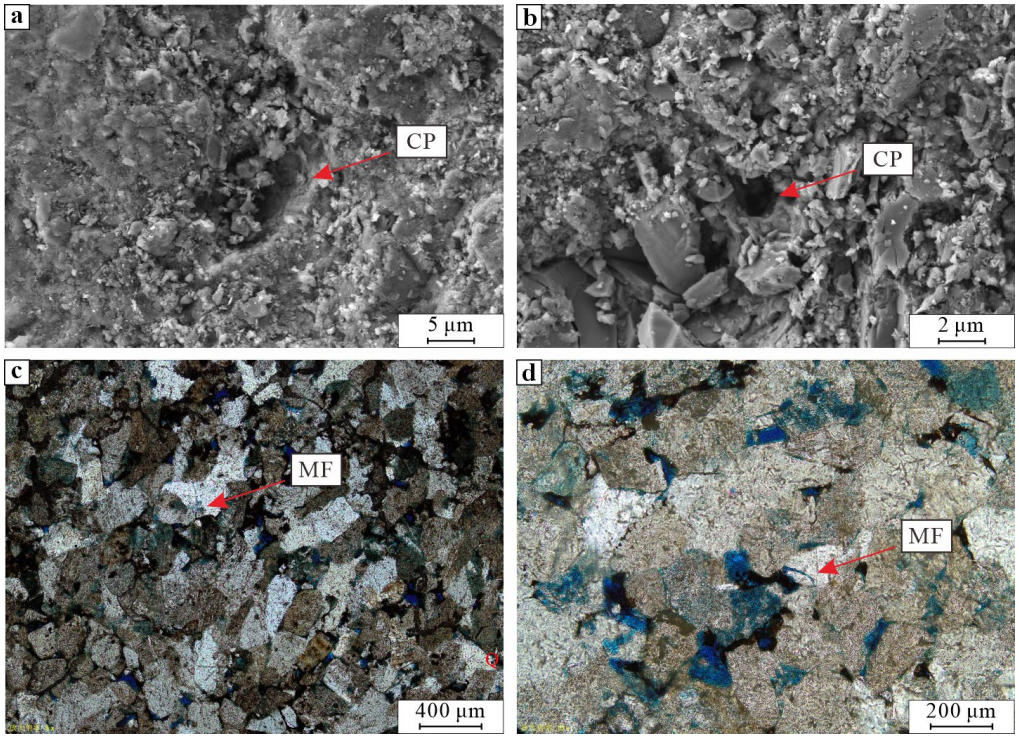



**Figure 6.** The development characteristics of clay mineral pores (CP) and microfractures (MF). (**a**,**b**) are intercrystalline pores of clay minerals; (**c**,**d**) are microfractures among brittle minerals.

### *3.3. Pore Size Distribution and Reservoir Classification*

The results of high-pressure mercury injection experiments were used to quantitatively characterize the pore size distribution of tight reservoirs, and based on the hysteresis loop characteristics between the advancing and retreating mercury curves, the connectivity of the pore structure was characterized (Figures 7 and 8). The displacement pressure ranged mainly from 0.4 to 7 MPa and was concentrated in the 1.0–3.0 MPa range, with a few samples exceeding 7.0 MPa (Figure 7). Correspondingly, nanoscale pores dominate the $Q_4$ reservoir, with the pore diameter lower than 700 nm. A total of 26 samples were tested, where the pore sizes of 18 samples were found to be lower than 1 μm (Figure 8). Consequently, the $Q_4$ reservoir in the study area was divided into three grades of I (average pore radius > 0.175 μm, porosity > 10%, and permeability > 0.25 mD), II (average pore radius: 0.075–0.175 μm, porosity: 8–10%, and permeability: 0.1–0.25 mD), and III (average pore radius < 0.075 μm, porosity < 8%, and permeability < 0.1 mD) according to the pore throat diameter, porosity, and permeability results in Lu's Classification (Table 2). For samples YX55-2, Y141-9, and G616-18 (Grade I reservoir), all of their mercury saturation rates were higher than 80% (Figure 7). In addition, their hysteresis loops are wide (larger than 50%), representing good pore connectivity. Samples YX55-3, YX55-4, and G616-20 have been categorized into the Grade II reservoir, and the mercury saturation ranged from 65% to 75% (Figure 7). In comparison, the hysteresis loops (40–50%) are narrower than in the Grade I reservoir, resulting relatively good pore connectivity. For the Grade III reservoir (samples YX55-8, YX55-9, and YX55-11), the mercury saturation was in the range of 40–50% (Figure 7), and the hysteresis loops are narrow, representing fair pore connectivity. Overall, the pore size distribution, pore volume, and pore connectivity of the Grade I reservoir are better than the Grade II and III reservoirs (Figures 7 and 8).

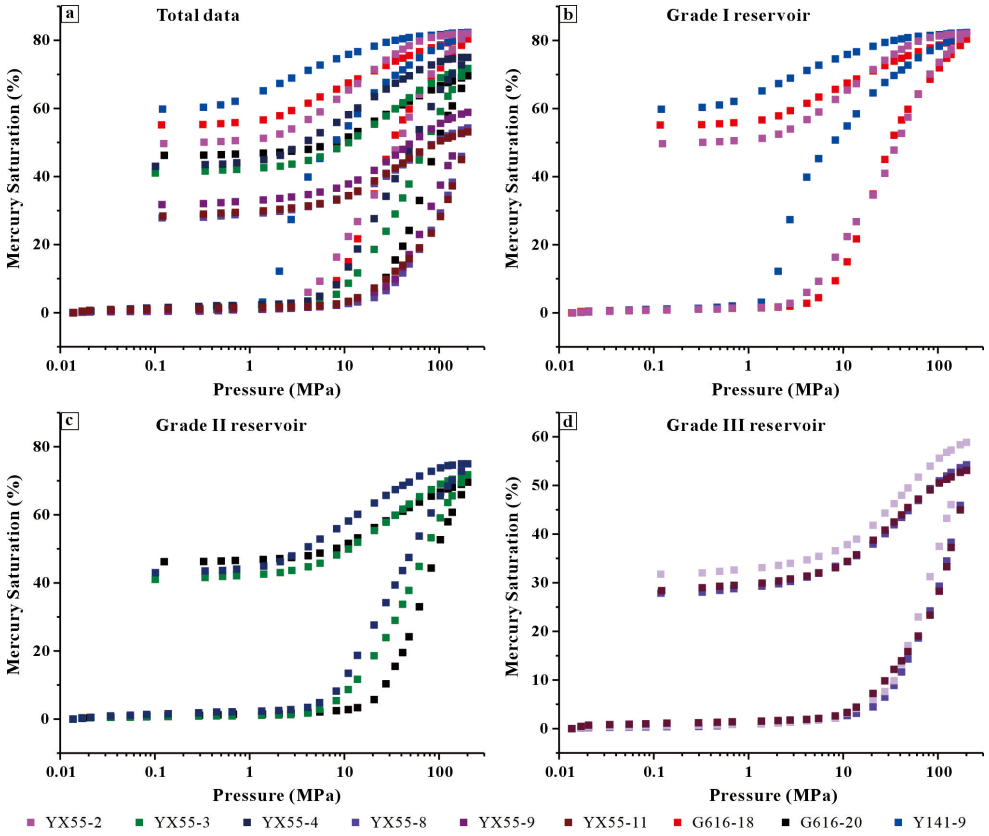



**Figure 7.** The advance and retreat mercury curves (**a**) of Grade I (**b**), II (**c**), and III (**d**) reservoirs in $Q_4$ reservoir.

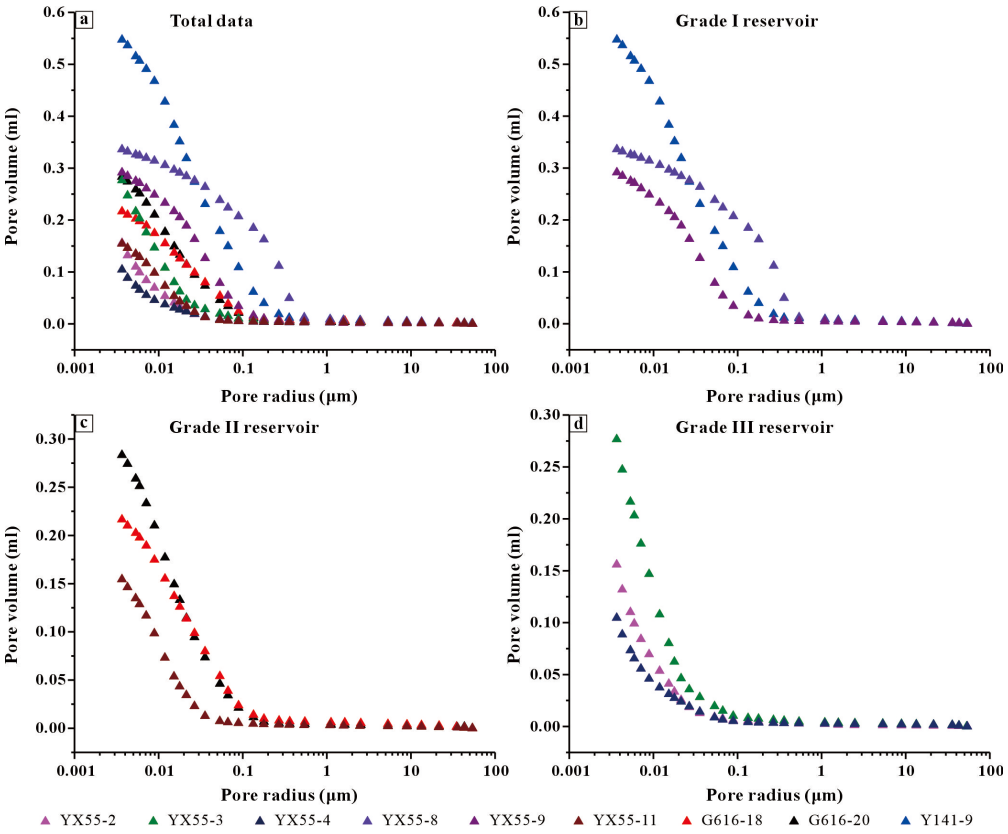



**Figure 8.** The pore size distribution curves (**a**) of Grade I (**b**), II (**c**), and III (**d**) reservoirs in $Q_4$ reservoir.

**Table 2.** The classification sand evaluation criteria for the $Q_4$ reservoir.

| Reservoir Grade | Average Pore Radius (μm) | Porosity (%) | Permeability (mD) |
|---|---|---|---|
| Grade I | >0.175 | >10 | >0.25 |
| Grade II | 0.075–0.175 | 8–10 | 0.1–0.25 |
| Grade III | <0.075 | <8 | <0.1 |

### *3.4. The Evolution Process and Mechanism of Pore Structure*

Based on the observation of microsection, electron probe, and scanning electron microscopy analysis (Figures 1–3, 5 and 6), the pore structure evolution of the $Q_4$ reservoir in the study area was subject to compaction, cementation, and dissolution during the diagenetic process. Original porosity maintenance and dissolution porosity increase are the positive factors for physical properties, whereas the compaction and cementation porosity decline are adverse effects (Table 3) [35–37]. Therefore, the impact of each diagenesis on porosity was calculated respectively according to Equations (1)–(7) (Table 3). To reveal the evolution stages and differential effects of various diagenesis on the pore structure of the $Q_4$ reservoir, the contributions of compaction, cementation, and dissolution on the porosity of the Grade I, II, and III reservoirs were calculated, respectively. The average original porosity of the Grade I reservoir is about 37.49%, and its compaction and cementation reduced to 24.92% and 2.67%, respectively, whereas the dissolution increased to 4.92%. As a result, the current porosity is 14.82%. For the Grade II reservoir, the original, compaction loss, cementation loss, and dissolution increase porosity are 36.58%, 23.48%, 7.33%, and 3.21%, respectively. Its current porosity is 8.98%. The cementation loss porosity for the Grade III reservoir is most serious, resulting in a reduction of 23.87% with a current porosity of only 3.57%.

**Table 3.** The evolution law of porosity in $Q_4$ tight reservoirs.

| Reservoir Type | Original Porosity (%) | Compaction Loss Porosity (%) | Cementation Loss Porosity (%) | Dissolution Increase Porosity (%) | Current Porosity (%) |
|---|---|---|---|---|---|
| Grade I | 37.49 | 24.92 | 2.67 | 4.92 | 14.82 |
| Grade II | 36.58 | 23.48 | 7.33 | 3.21 | 8.98 |
| Grade III | 36.92 | 23.87 | 12.04 | 2.56 | 3.57 |

(1) Pore evolution of Grade I reservoir

The $Q_4$ reservoir is at the middle diagenetic stage now, having gone through the early diagenetic stage, as well as periods A and B of the middle diagenetic stage. At the early diagenetic stage, compaction dominated the pore evolution. Mineral particles in the reservoir were compressed with the gradual increase in formation pressure, causing a rapid decrease in the original porosity and permeability of the reservoir (Figure 9). Moreover, the early cementation led to the precipitation and attachment of some cements such as carbonates and silicates between mineral particles, changing the connection mode and contact relationship between particles, further squeezing the pore space, reducing the primary pores, and decreasing the porosity. At the A period of the middle diagenetic stage, the early cement and matrix altered the contact mode between particles obviously. Smectite gradually loosed interlayer water and transformed into illite through a series of complex physical and chemical processes [38,39]. In addition, the strong dissolution of feldspar under the action of acidic pore fluids was an important factor in improving the physical properties of the reservoir. Secondary pores were formed in this process, increasing the porosity. However, if the dissolution products cannot be carried away by the pore fluid in a timely manner, they may re-precipitate in situ and participate in cementation, which is detrimental to the development of reservoir properties. Meanwhile, the early

cementation filled some pores and further reduced porosity. On the other hand, it also plays a supporting role in mineral particles to a certain extent, preventing excessive compaction during subsequent diagenesis and buffering the decrease in permeability. At the B period of the middle diagenetic stage, a small amount of late stage cement appeared. Due to the weak cementation of Grade I reservoirs, which causes minimal damage to the porosity and has undergone strong dissolution and transformation, the overall physical properties of this type of reservoir are good.

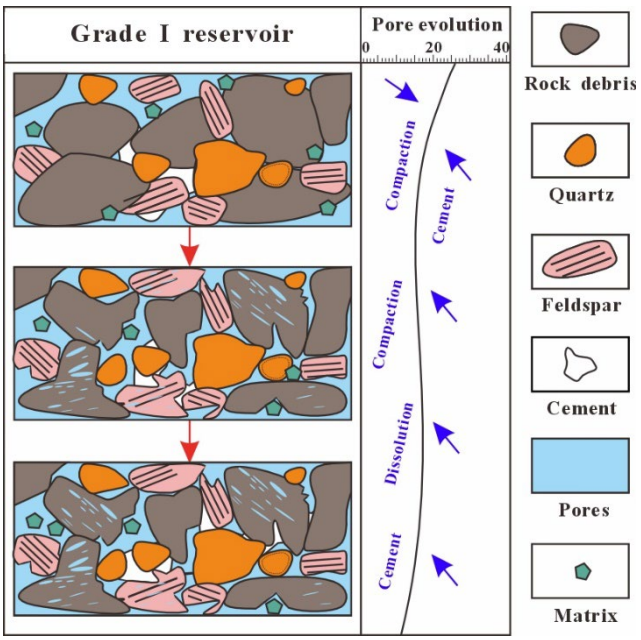



**Figure 9.** The pore evolution pattern of Grade I reservoir.

(2) Pore evolution of Grade II reservoir

At the early diagenetic stage of the Grade II reservoir, compaction was also the main reason for the serious porosity reduction, resulting in the deterioration of accumulation properties. Early cementation began to manifest at the A period of the middle diagenetic stage, where partial cements such as carbonates and siliceous began to precipitate and precipitate between mineral particles, further squeezing the pore space and leading to a decrease in porosity (Figure 10). Meanwhile, under the synergistic effect of a specific temperature, pressure, and pore fluid environment, clay minerals continuously underwent transformation. Moreover, the dissolution of feldspar contributed positively to improving the reservoir performance, but the dynamic balance between dissolution and cementation largely led to complex changes in the physical properties of the Grade II reservoir during the middle diagenetic stage. Late-stage cements of iron bearing carbonates and silicates began to largely form at the B period of the middle diagenetic stage, which further exacerbated the reduction in pore space. Additionally, the continuous compaction effect was still strong, the mineral particles were arranged more tightly, and the porosity and permeability continued to decrease. Overall, the cementation effect of Grade II reservoirs is moderate and causes strong damage. However, due to their strong dissolution transformation, the physical properties of this type of reservoir are only followed by Grade I reservoirs.

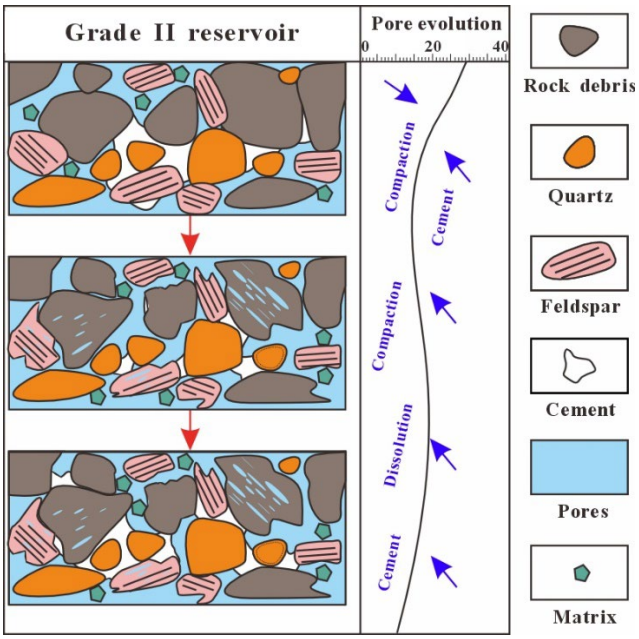



**Figure 10.** The pore evolution pattern of Grade II reservoir.

(3) Pore evolution of Grade III reservoir

The pores of the Grade III reservoir have three different evolutionary characteristics: the type I reservoir initially underwent weak dissolution and then underwent strong calcareous cementation; the type II reservoir experienced strong cementation in the early stage, but the dissolution could be neglected; matrix filling dominated the early stages of type III reservoir, and no obvious dissolution occurred in the late stages (Figures 11–13). A large amount of calcite cement is the main feature of type I reservoirs, and basal cementation dominates its structure with poor physical properties. The compaction in the early diagenetic stage was compaction that led to the arrangement of mineral particles that gradually shifted from loose to tight, and the pore space was significantly reduced. The original porosity and permeability of the reservoir decreased sharply, resulting in initial deterioration of its reservoir performance. During diagenetic stage A, carbonate and siliceous cement begin to precipitate and precipitate between mineral particles, further squeezing the pore space and reducing porosity. Meanwhile, montmorillonite and kaolinite undergo transformation under conditions of increased temperature and pressure. During the A period of the middle diagenetic stage, carbonate and siliceous cements began to precipitate and precipitate between mineral particles, further squeezing the pore space and reducing porosity. Meanwhile, smectite and kaolinite underwent continuous transformation. The further strengthening of cementation and continuous compaction in the B period of the middle diagenetic stage led to a tighter arrangement of minerals, resulting in a significant decrease in reservoir porosity and permeability.

Compaction and cementation were the dominant diagenesis processes in this type of reservoir at the early diagenetic stage. In comparison, the porosity reductions of cementation in the type II reservoir were stronger than that in the type I reservoir, and a large amount of cement was filled in the pores, causing a sharp deterioration of the reservoir properties (Figure 12). Meanwhile, compaction was also the most important reason for porosity evolution, as well as that in the above reservoirs. At the middle diagenetic stage, the cements formed at the early diagenetic stage still blocked the pores, and the compaction effect became stronger, further reducing the accumulation space. This blocking also greatly limited the flow ability of fluids in reservoirs, resulting in the inability of diagenetic fluids

to enter the interior of the reservoir in the later stage, and thus the physical properties could not be improved. Therefore, the mining value of this type of reservoir is worse.

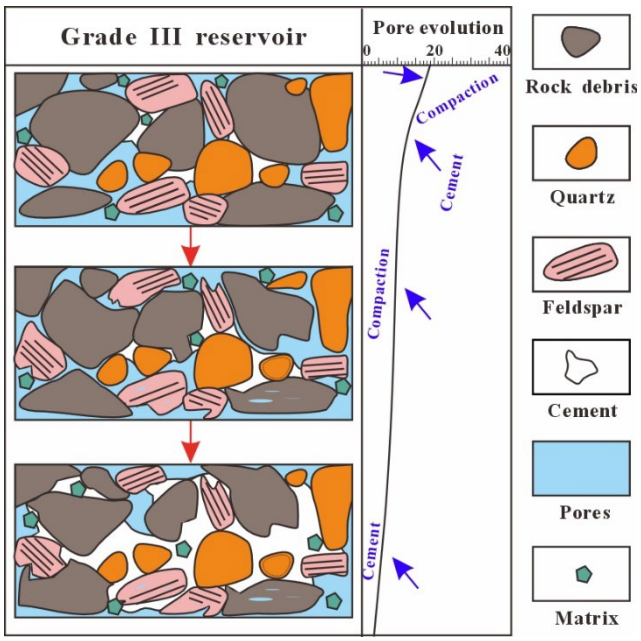



**Figure 11.** The pore evolution pattern of Grade III (type I) reservoir.

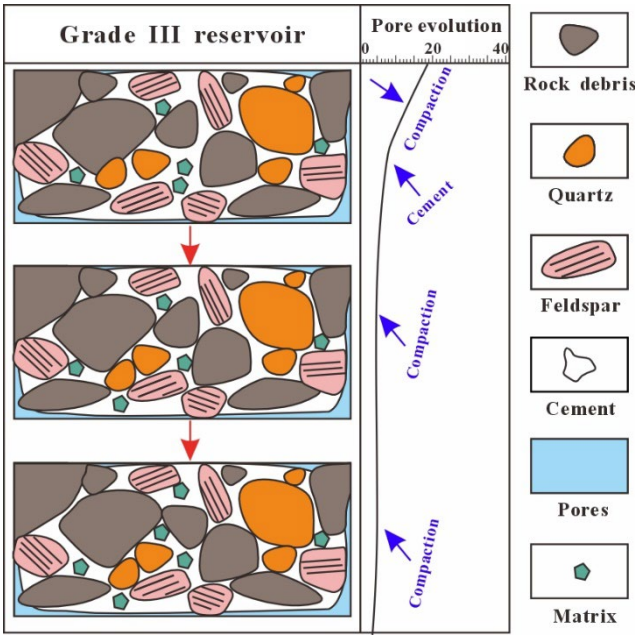



**Figure 12.** The pore evolution pattern of Grade III (type II) reservoir.

In the type III reservoir, a large amount of clay mineral matrix filling pores is an important reason for the deterioration of reservoir properties in addition to compaction, which is different from types I and II reservoir (Figure 13). Therefore, matrix filling and compaction dominated the early diagenetic stage. At the middle diagenetic stage, feldspar, rock debris, and other easily soluble components were transformed to new authigenic clay minerals, which further filled the pores. Meanwhile, the compaction became stronger with deeper burial depth, causing a continuous decrease in porosity. Similar to the type II reservoir, the precipitate and accumulation of the matrix in the pores limited the improvement of reservoir properties by later diagenetic fluids. As a result, the type of reservoir was deemed as strategic reserve resources.

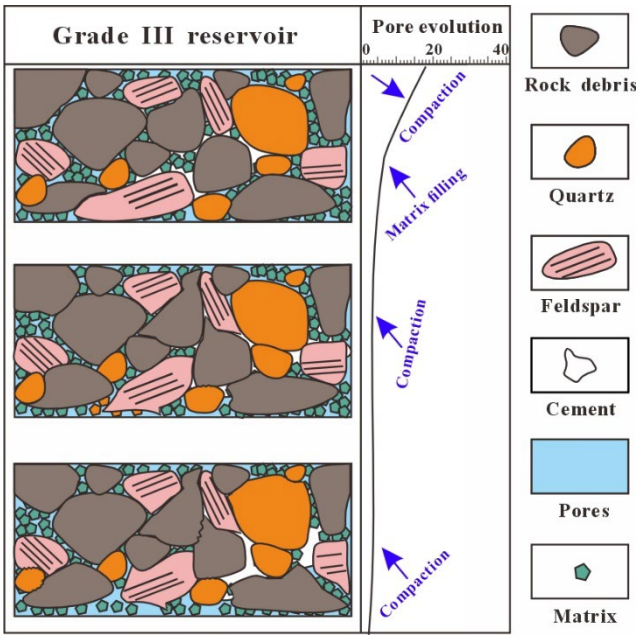



**Figure 13.** The pore evolution pattern of Grade III (type III) reservoir.

Overall, the physical properties of the Grade I reservoirs in the research area are the best, with weak cementation and strong dissolution during diagenesis. Both their pore structure and connectivity are considerable, and the hydraulic fracturing stimulation could easy communicate with the microscopic pore structure system, effectively ehhancing recovery. Although the middle cementation and dissolution lead to relatively worse physical properties of Grade II reservoirs than Grade I reservoirs, these are also deemed as the favorable reservoirs. However, Grade III reservoirs experienced strong cementation and weak dissolution, resulting in poor pore structure and connectivity. In addition, their clay matrix content is relatively high, meaning that conventional hydraulic fracturing may be difficult to effectively increase recovery due to the water sensitivity of clay minerals. Anhydrous fracturing of supercritical $CO_2$ is a potential scheme for increasing production.

## 4. Conclusions

(1) The $Q_4$ tight reservoir is composed only of siltstone and pelitic siltstone; feldspar and quartz are the main rock-forming minerals, also including also a certain amount of rock debris. The lithology includes rock debris–feldspar siltstone, feldspar–rock debris siltstone, and rock debris siltstone. Among them, the content of potassium feldspar is larger than plagioclase, and the content of igneous debris is larger than metamorphic debris.

(2) Intergranular pores, intergranular dissolution pores, intragranular dissolution pores, intercrystalline pores, and microfractures are widely developed in the $Q_4$ reservoir, with a porosity of 4% to 12% and a permeability 0.001 to 1 mD, which belongs to low porosity and ultralow permeability reservoirs. The pore diameter of the $Q_4$ reservoir is mostly lower than 1 μm, and it was divided into three grades of I, II, and II from good to poor according to their, porosity, permeability, and pore size distribution.

(3) The Grade I reservoir has the best mining potential; its original porosity is about 37.49%, its compaction and cementation reduced to 24.92% and 2.67%, respectively, whereas its dissolution increased to 4.92%. For the Grade II reservoir, the original, compaction loss, cementation loss, and dissolution increase porosity are 36.58%, 23.48%, 7.33%, and 3.21%, respectively. The cementation loss porosity for the Grade III reservoir is most serious, resulting in a reduction of 23.87%, with a current porosity of only 3.57%.

This work evaluated the Q4 reservoir into three grades based on the physical properties and diagenetic evolution process, which has certain theoretical significance for the deployment of exploration and development work. It should be noted that the research results are mainly qualitative analysis, which was subjected to the limited sample amount and evaluation indicators. Further work will focus on the planar variation of its physical properties in the study area and conduct a quantitative evaluation of the reservoir quality.

**Author Contributions:** Scientific literature collection and data analysis, Q.W., J.H., and Y.Z.; writing and revision, J.L., F.C., and Q.Z. All authors have read and agreed to the published version of the manuscript.

**Funding:** This research was funded by [National Natural Science Foundation of China] grant number [U19B2007].

**Data Availability Statement:** The data presented in this study are available upon request from the corresponding author.

**Conflicts of Interest:** Authors Junhui Li, Fangju Chen, Qiang Zheng, Yanping Zhu, Qi Wang and Jiawei Hao were employed by PetroChina Daqing Oilfield Company. The authors declare that the research was conducted in the absence of any commercial or financial relationships that could be construed as a potential conflict of interest.

## References

1. Wachtmeister, H.; Höök, M. Investment and production dynamics of conventional oil and unconventional tight oil: Implications for oil markets and climate strategies. *Energy Clim. Change* **2020**, *1*, 100010. [CrossRef]
2. Boak, J.; Kleinberg, R. Shale gas, tight oil, shale oil and hydraulic fracturing. In *Future Energy*; Elsevier: Amsterdam, The Netherlands, 2020; pp. 67–95. [CrossRef]
3. Xie, W.; Chen, S.; Gan, H.; Wang, H.; Wang, M.; Vandeginste, V. Preservation conditions and potential evaluation of the Longmaxi shale gas reservoir in the Changning area, southern Sichuan Basin. *Geosci. Lett.* **2023**, *10*, 36. [CrossRef]
4. Kabir, S.; Rasdi, F.; Igboalisi, B. Analyzing production data from tight oil wells. *J. Can. Pet. Technol.* **2011**, *50*, 48–58. [CrossRef]
5. Aguilera, R. Flow units: From conventional to tight-gas to shale-gas to tight-oil to shale-oil reservoirs. *SPE Reserv. Eval. Eng.* **2014**, *17*, 190–208. [CrossRef]
6. Xie, W.; Wang, H.; Vandeginste, V.; Chen, S.; Gan, H.; Wang, M.; Yu, Z. Thermodynamic and kinetic affinity of $CO_2$ relative to $CH_4$ and their pressure, temperature and pore structure sensitivity in the competitive adsorption system in shale gas reservoirs. *Energy* **2023**, *277*, 127591. [CrossRef]
7. Zhou, Q.; Li, X.; Qian, Z.; Chen, G.; Lyu, C.; Ma, X.; Li, C. The occurrence of adsorbed tight oil and its effect on porosity and permeability reduction of Triassic lacustrine sandstone reservoir. *Geofluids* **2022**, *2022*, 6923449. [CrossRef]
8. Sun, Y.P.; Xin, Y.; Lyu, F.T.; Dai, C.L. Experimental study on the mechanism of adsorption-improved imbibition in oil-wet tight sandstone by a nonionic surfactant for enhanced oil recovery. *Pet. Sci.* **2021**, *18*, 1115–1126. [CrossRef]
9. Ran, Y.; Du, C.; Zhang, J. Accumulation condition of "below the source rock" tight oil in the 4th member of Cretaceous Quantou Formation in Putaohua Oilfield, northern Songliao Basin. *Lithol. Reserv.* **2025**, *37*, 47–58. [CrossRef]
10. Liu, Q.; Zhang, Y. Diagenesis and diagenetic facies of extra-low to ultra-low permeability reservoir in the Member 4 of Quantou Formation in Yudong area, Songliao Basin. *J. Palaeogeogr.* **2025**, *27*, 499–516. [CrossRef]
11. Xi, K.; Cao, Y.; Jahren, J.; Zhu, R.; Bjørlykke, K.; Haile, B.G.; Zheng, L.; Hellevang, H. Diagenesis and reservoir quality of the Lower Cretaceous Quantou Formation tight sandstones in the southern Songliao Basin, China. *Sediment. Geol.* **2015**, *330*, 90–107. [CrossRef]
12. Huang, W.; Lu, S.; Osman, S.H. Quality grading system for tight sandstone reservoirs in the Quantou 4 Member, southern Songliao Basin, Northeast China. *Interpretation* **2017**, *5*, T503–T522. [CrossRef]
13. Ma, C.; Liu, C.; Zhou, X.; Tang, J.J.; Liu, Y.L. Microscopic pore structure of dense sandstone reservoirs and its influence on movable fluids: A case study from the fourth Member of Quantou Formation in the Central Depression, Songliao Basion. *J. Yangtze Univ. (Nat. Sci. Ed.)* **2025**. [CrossRef]
14. Zhang, Q.; Wu, X.S.; Radwan, A.E.; Wang, B.-H.; Wang, K.; Tian, H.-Y.; Yin, S. Diagenesis of continental tight sandstone and its control on reservoir quality: A case study of the Quan 3 member of the cretaceous Quantou Formation, Fuxin uplift, Songliao Basin. *Mar. Pet. Geol.* **2022**, *145*, 105883. [CrossRef]
15. Zhang, Q.; Zhang, Y.X.; Wang, B.H.; Yin, S.; Wu, X.S.; Yuan, C.S. Comprehensive evaluation and reservoir classification in the Quan 3 member of the Cretaceous Quantou Formation in the Fuxin Uplift, Songliao Basin. *Front. Earth Sci.* **2022**, *10*, 1016924. [CrossRef]

16. Cao, Z.; Lin, C.; Dong, C.; Ren, L.; Han, S.; Dai, J.; Xu, X.; Qin, M.; Zhu, P. Impact of sequence stratigraphy, depositional facies, diagenesis and $CO_2$ charge on reservoir quality of the lower cretaceous Quantou Formation, Southern Songliao Basin, China. *Mar. Pet. Geol.* **2018**, *93*, 497–519. [CrossRef]
17. Zhao, Y.; Wu, S.; Chen, Y.; Yu, C.; Yu, Z.; Hua, G.; Guan, M.; Lin, M.; Yu, X. $CO_2$-water-rock interaction and pore structure evolution of the tight sandstones of the Quantou formation, Songliao Basin. *Energies* **2022**, *15*, 9268. [CrossRef]
18. Li, L.; Li, Z.; Han, H.; Liu, C.; Li, Y.; Zhao, W.; Wang, J.; Bao, Z. Multifractal Analysis of Tight Sandstone Using Micro-CT Methods: A Case from the Lower Cretaceous Quantou Formation, Southern Songliao Basin, NE China. *Fractal Fract.* **2025**, *9*, 336. [CrossRef]
19. Yang, Z.; Tang, X.; Xiao, H.; Zhang, F.; Jiang, Z.; Liu, G. Water film thickness of tight reservoir in Fuyu oil layer of Cretaceous Quantou Formation in Songliao Basin and its influence on the lower limit of seepage. *Mar. Pet. Geol.* **2022**, *139*, 105592. [CrossRef]
20. Shen, H.; Yang, L.; Han, H.; Wang, Y.; Xing, J.; Xue, S.; Liu, H. New fields, new types and resource potentials of oil-gas exploration in southern Songliao Basin. *Acta Pet. Sin.* **2023**, *44*, 2104–2121. [CrossRef]
21. Wang, X.; Bai, X.; Lu, J.; Jin, Z.; Wang, G.; Kuang, L.; Li, J.; Li, J.; Zhang, J.; Sun, L.; et al. New fields, new types and resource potentials of oil-gas exploration in northern Songliao Basin. *Acta Pet. Sin.* **2023**, *44*, 2091–2103+2178. [CrossRef]
22. Beard, D.C.; Weyl, P.K. Influence of texture on porosity and permeability of unconsolidated sand. *AAPG Bull.* **1973**, *57*, 349–369. [CrossRef]
23. Sun, M.; Liu, C.; Yang, Y.; Feng, C. Origin and classification of the composite sand bodies of the delta front in K1q4 of the Quantou Formation in the central region of the Fuyu oil field. *J. Pet. Explor. Prod. Technol.* **2016**, *6*, 629–639. [CrossRef]
24. Luo, C.; Jia, A.; Guo, J.; Liu, W.; Yin, N.; Chen, C.; Wang, J.; Gao, X.; Guo, Z. Modeling of dense well block point bar architecture based on geological vector information: A case study of the third member of Quantou Formation in Songliao Basin. *Open Geosci.* **2021**, *13*, 39–48. [CrossRef]
25. Gao, Y.; Wang, Z.; She, Y.; Lin, S.; Lin, M.; Zhang, C. Mineral characteristic of rocks and its impact on the reservoir quality of He 8 tight sandstone of Tianhuan area, Ordos Basin, China. *J. Nat. Gas Geosci.* **2019**, *4*, 205–214. [CrossRef]
26. Liu, Y.; Zhang, X.; Shi, J.; Guo, W.; Kang, L.; Yu, R.; Sun, Y.; Wang, Z.; Pan, M. A reservoir quality evaluation approach for tight sandstone reservoirs based on the gray correlation algorithm: A case study of the Chang 6 layer in the W area of the as oilfield, Ordos Basin. *Energy Explor. Exploit.* **2021**, *39*, 1027–1056. [CrossRef]
27. Xie, W.; Wang, M.; Wang, H.; Ma, R.; Duan, H. Diagenesis of shale and its control on pore structure, a case study from typical marine, transitional and continental shales. *Front. Earth Sci.* **2021**, *15*, 378–394. [CrossRef]
28. Xie, W.; Chen, S.; Vandeginste, V.; Yu, Z.; Wang, H.; Wang, M. Review of the effect of diagenetic evolution of shale reservoir on the pore structure and adsorption capacity of clay minerals. *Energy Fuels* **2022**, *36*, 4728–4745. [CrossRef]
29. Qiao, J.; Zeng, J.; Jiang, S.; Feng, S.; Feng, X.; Guo, Z.; Teng, J. Heterogeneity of reservoir quality and gas accumulation in tight sandstone reservoirs revealed by pore structure characterization and physical simulation. *Fuel* **2019**, *253*, 1300–1316. [CrossRef]
30. Zhu, P.; Dong, Y.; Chen, M.; Li, Z.; Han, B.; Wang, J.; Cui, Y. Quantitative evaluation of pore structure from mineralogical and diagenetic information extracted from well logs in tight sandstone reservoirs. *J. Nat. Gas Sci. Eng.* **2020**, *80*, 103376. [CrossRef]
31. Sima, L.; Wang, C.; Wang, L.; Wu, F.; Ma, L.; Wang, Z. Effect of pore structure on the seepage characteristics of tight sandstone reservoirs: A case study of Upper Jurassic Penglaizhen Fm reservoirs in the western Sichuan Basin. *Nat. Gas Ind. B* **2017**, *4*, 17–24. [CrossRef]
32. Qu, H.J.; Yang, B.; Tian, X.H.; Liu, X.-S.; Yang, H.; Dong, W.-W.; Chen, Y.-H. The primary controlling parameters of porosity, permeability, and seepage capability of tight gas reservoirs: A case study on Upper Paleozoic Formation in the eastern Ordos Basin, Northern China. *Pet. Sci.* **2019**, *16*, 1270–1284. [CrossRef]
33. Lai, J.; Wang, G.; Ran, Y.; Zhou, Z.; Cui, Y. Impact of diagenesis on the reservoir quality of tight oil sandstones: The case of Upper Triassic Yanchang Formation Chang 7 oil layers in Ordos Basin, China. *J. Pet. Sci. Eng.* **2016**, *145*, 54–65. [CrossRef]
34. Mustafa, A.; AMahmoud, M.; Abdulraheem, A. A review of pore structure characterization of unconventional tight reservoirs. In Proceedings of the Abu Dhabi International Petroleum Exhibition and Conference, Abu Dhabi, United Arab Emirates, 11–14 November 2019; p. D031S098R001. [CrossRef]
35. Mills, M.M.; Sanchez, A.C.; Boisvert, L.; Payne, C.B.; Ho, T.A.; Wang, Y. Understanding smectite to illite transformation at elevated (>100 C) temperature: Effects of liquid/solid ratio, interlayer cation, solution chemistry and reaction time. *Chem. Geol.* **2023**, *615*, 121214. [CrossRef]
36. Lander, R.H.; Walderhaug, O. Predicting porosity through simulating sandstone compaction and quartz cementation. *AAPG Bull.* **1999**, *83*, 433–449. [CrossRef]
37. Yue, D.; Wu, S.; Xu, Z.; Xiong, L.; Chen, D.; Ji, Y.; Zhou, Y. Reservoir quality, natural fractures, and gas productivity of upper Triassic Xujiahe tight gas sandstones in western Sichuan Basin, China. *Mar. Pet. Geol.* **2018**, *89*, 370–386. [CrossRef]

38. Shao, X.; Pang, X.; Jiang, F.; Li, L.; Huyan, Y.; Zheng, D. Diagenetic characteristics and reservoir quality in tight gas sandstones: A case study of the Shanxi Formation in the north--eastern Ordos Basin, China. *Geol. J.* **2019**, *54*, 3257–3271. [CrossRef]
39. Xie, W.; Wang, M.; Chen, S.; Vandeginste, V.; Yu, Z.; Wang, H. Effects of gas components, reservoir property and pore structure of shale gas reservoir on the competitive adsorption behavior of $CO_2$ and $CH_4$. *Energy* **2022**, *254*, 124242. [CrossRef]

**Disclaimer/Publisher's Note:** The statements, opinions and data contained in all publications are solely those of the individual author(s) and contributor(s) and not of MDPI and/or the editor(s). MDPI and/or the editor(s) disclaim responsibility for any injury to people or property resulting from any ideas, methods, instructions or products referred to in the content.